Available online at www.sciencedirect.com
ScienceDirect
Polymer 47 (2006) 6814–6825
polymer
www.elsevier.com/locate/polymer

Star-shaped poly(ε-caprolactone) with polyhedral oligomeric silsesquioxane core

Yonghong Liu, Xingtian Yang, Weian Zhang, Sixun Zheng*

Department of Polymer Science and Engineering, Shanghai Jiao Tong University, 800 Dongchuan Road, Shanghai 200240, PR China

Received 23 March 2006; received in revised form 28 June 2006; accepted 23 July 2006
Available online 14 August 2006

Abstract

A readily available octa(3-chloropropyl) polyhedral oligomeric silsesquioxane (POSS) [$(ClCH_2CH_2CH_2)_8Si_8O_{12}$] framework was used to prepare octa(3-hydroxypropyl) POSS [$(HOCH_2CH_2CH_2)_8Si_8O_{12}$], which was further used as an initiator to synthesize star poly(ε-caprolactone) with POSS core *via* ring-opening polymerization catalyzed by Stannous (II) octanoate [$Sn(Oct)_2$]. The organic–inorganic star PCLs were characterized by means of gel permeation chromatograph (GPC), Fourier transform infrared spectroscopy (FTIR) and nuclear magnetic resonance spectroscopy (NMR). The wide-angle X-ray diffraction (WAXRD) experiments indicate that the presence of POSS cores did not alter the crystal structure of PCL. The star PCLs exhibited enhanced melting temperatures in comparison with the linear counterpart. The isothermal crystallization kinetics shows that both the overall crystallization rate and the spherulitic growth rate of the star PCLs increased with increasing the concentration of POSS (or with decreasing the arm lengths of the stars). The fold surface free energy of the star PCLs decreased with increasing the concentration of POSS. These results could be interpreted based on the effect of the heterogeneous nucleation of POSS cores, which accelerates the process of crystallization.

Keywords: Synthesis; Star poly(ε-caprolactone); Polyhedral oligomeric silsesquioxane (POSS)

1. Introduction

Star polymers have attracted considerable attention in recent years due to their branched structures and unique physicochemical properties different from those of their linear counterparts [1,2]. The syntheses of star polymers can generally be divided into two routes. The first one is called arm-first approach, *i.e.*, the pre-prepared macromolecular chains (*viz.* arms) are coupled with multifunctional cores to afford hetero-armed or miktoarmed star polymers [3–7]. The second one is core-first technique, in which multifunctional compounds are used to initiate the polymerization of monomers. Core-first approach has been proved to be efficient to prepare a series of well-defined star polymers with precise arm numbers and lengths *via* living polymerization techniques such as atomic transfer radical polymerization (ATRP) [8–18], reversible radical fragment transfer (RAFT) [19] and ring-opening polymerization (ROP) [20,21].

Aliphatic polyesters such as poly(ε-caprolactone) (PCL) and poly(lactide) (PLA) are a class of important polymer materials. Owing to their degradability and biocompatibility, these polymers represent a class of interesting candidates for environmentally benign packing materials [22–27] and for biomedical applications [28]. Recently, the aliphatic polyesters with well-defined architectures such as dendritic, star-shaped macromolecular topologies are attracting considerable interests due to the special properties in comparison with their linear homologues. Some investigators have synthesized the star-shaped poly(ε-caprolactone) with different number of arms using a variety of organic core initiators [25,29–32].

* Corresponding author. Tel.: +86 21 54743278; fax: +86 21 54741297.
E-mail address: szheng@sjtu.edu.cn (S. Zheng).

0032-3861/$ - see front matter © 2006 Elsevier Ltd. All rights reserved.
doi:10.1016/j.polymer.2006.07.050

All the previous studies have dealt with the synthesis of star PCL with organic core initiators. However, organic–inorganic star-shaped PCLs with inorganic cores remain largely unexplored. Polyhedral clusters containing silicon and oxygen such as spherosilicates [33] and polyhedral oligomeric silsesquioxane (POSS) [34] are a class of versatile building blocks to access inorganic–organic hybrid materials with designed properties due to their well-defined stereo structures [35]. Spherosilicates are often prepared by silylation of silicate solution [36,37] whereas POSS is obtained from hydrolytic condensation reaction of trifunctional organosilanes. During the past years, polyhedral oligomeric silsesquioxane (POSS) has emerged as a new class of nanofillers for the preparation of higher-performance nanostructured organic–inorganic composites [38,39] in comparison with other inorganic nanofillers [40–45]. A typical POSS molecule possesses the structure of cube-octameric frameworks represented by the formula ($R_8Si_8O_{12}$) with an inorganic silica-like core (Si_8O_{12}) (~0.53 nm in diameter) surrounded by eight organic corner groups, one or more of which are reactive (Scheme 1). Octafunctional POSS molecules are ideal nanosized starting materials for the syntheses of inorganic–organic hybrid octaarmed star-shaped polymers [6,7].

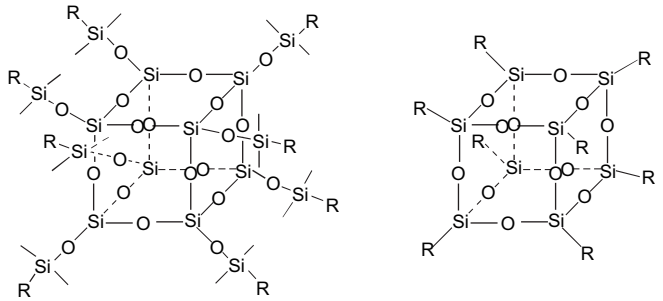

Scheme 1. Structures of spherosilicates (A) and POSS (B). R = organic groups.

In this contribution, we proposed a new and facile approach to prepare octa(3-hydroxypropyl) silsesquioxane from readily available octa(3-chloropropyl) polyhedral oligomeric silsesquioxane. The octahydroxyl-functionalized POSS molecule was used as an initiator for preparing octaarmed star-shaped PCLs *via* ring-opening polymerization (see Scheme 2). The goal of this work is to report the synthesis of the star-shaped PCL with POSS core with high molecular weights and to investigate the thermal properties and crystallization behavior of the star PCLs. The organic–inorganic star PCLs were characterized by Fourier transform infrared (FTIR) and nuclear magnetic resonance spectroscopy (NMR). X-ray diffraction analysis (XRD) was used to investigate the crystal structure of the star PCL. In the mean time, the crystallization and melting behavior of the hybrid PCLs were addressed on the basis of differential scanning calorimetry (DSC).

2. Experimental

2.1. Materials

3-Chloropropyltrimethoxysilane [$ClC_3H_6Si(OCH_3)_3$, 98%] was kindly supplied by Guotai Huarong Chemical Co., Jiangsu, China and was used as received. The monomer, ε-caprolactone was purchased from Fluka Co. Germany and it was distilled over CaH_2 under decreased pressure prior to use. A linear poly(ε-caprolactone) (PCL) was obtained from Solvay Chemical Co., UK and it has a quoted molecular weight of $M_n = 50{,}000$. Stannous (II) octanoate [$Sn(Oct)_2$] is of analytical grade and was purchased from Shanghai Reagent Co., China, and was used without further purification. Toluene was purified by distillation over CaH_2. Petroleum ether (distillation range: 60–90 °C) and dichloromethane were used without further purification. Silver nitrate ($AgNO_3$), sodium hydroxide (NaOH), ethanol and tetrahydrofuran were obtained from Shanghai Reagent Co., Shanghai, China.

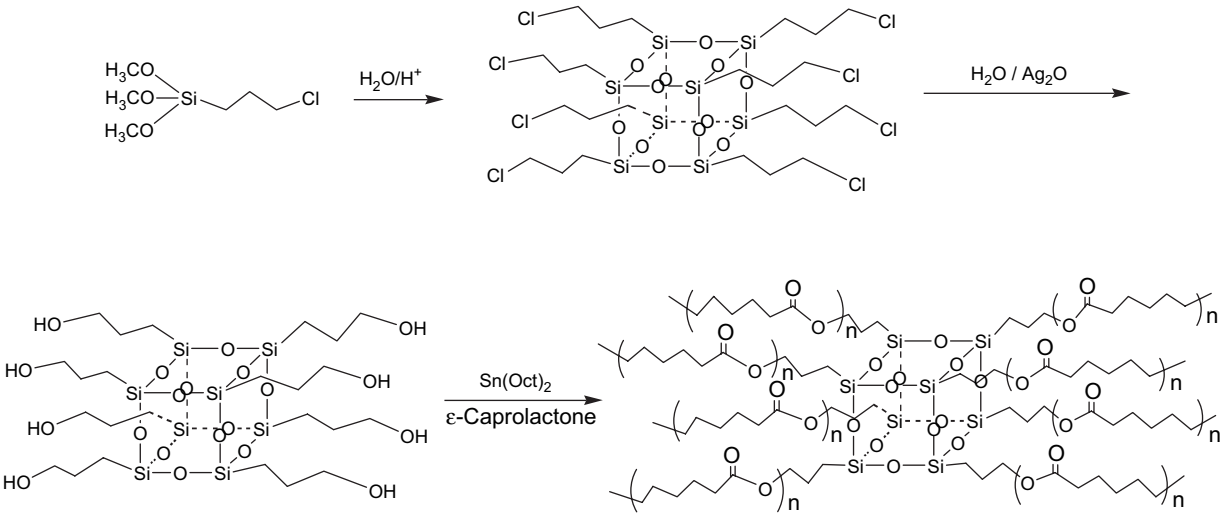

Scheme 2. Synthetic route of star PCLs with POSS core.

2.2. Synthesis of octa(3-chloropropyl) POSS [$(ClC_3H_6)_8Si_8O_{12}$]

Octa(3-chloropropyl) POSS [$(ClCH_2CH_2CH_2)_8Si_8O_{12}$] was synthesized by following the method described by Dittmar et al. [47]. Typically, 1800 ml methanol, 79.5 g (0.4 mol) 3-chloropropyltrimethoxysilane, 90 ml concentrated hydrochloric acid were mixed and the hydrolysis and rearrangement reactions were allowed to carry out for at least 5 weeks and 14.3 g (yield: 31.2%) colorless crystals were obtained after dried *in vacuo* at 60 °C for 48 h. FTIR (KBr window, cm^{-1}): 2984, 2954, 2872 (ν_{C-H}); 1109 ($\nu_{Si-O-Si}$), 759 (ν_{C-Cl}). ^1H NMR (DMSO-d_6, ppm): 3.58–3.62 (m, $SiCH_2CH_2CH_2Cl$, 2.3*H*); 1.73–1.80 (m, $SiCH_2CH_2CH_2Cl$, 2.2*H*); 0.75–0.79 (m, $SiCH_2CH_2CH_2OH$, 2.0*H*). ^{13}C NMR (DMSO-d_6, ppm): 9.6 ($SiCH_2CH_2CH_2Cl$); 26.5 ($SiCH_2CH_2CH_2Cl$); 47.3 ($SiCH_2CH_2CH_2Cl$). ^{29}Si NMR (ppm): −65.6, −66.3.

2.3. Synthesis of octa(3-hydroxypropyl) POSS [$(HOC_3H_6)_8Si_8O_{12}$]

Octa(3-hydroxypropyl) POSS was prepared by the hydrolysis of octa(3-chloropropyl) POSS in the presence of fresh silver oxide (Ag_2O). Firstly, the Ag_2O was prepared. In a typical experiment, $AgNO_3$ (1.57 g, 9.3 mmol) was dissolved in 10 ml of deionized water and aqueous NaOH (0.37 g, 9.3 mmol) was slowly dropped into the solution with vigorous stirring. The silver oxide precipitates were isolated and washed with deionized water for three times. After that, to a round-bottomed flask, octa(3-chloropropyl) POSS (1.0 g, 0.96 mmol), ethanol (25 ml) and tetrahydrofuran (25 ml) were charged to afford a transparent solution and then the above newly prepared Ag_2O together with 1 ml of deionized water was added to the system. The reactive system was refluxed in the dark with vigorously stirring for 48 h. The insolubilities were filtered out and the solution was subjected to rotary evaporation to obtain white solids (0.78 g) with a yield of 91%. FTIR (KBr, cm^{-1}): 3436 cm^{-1} (−OH); 1109 (Si−O−Si). ^1H NMR (DMSO-d_6, ppm): 3.58–3.62 (m, $SiCH_2CH_2CH_2OH$, 16.3*H*); 3.39 (s, $SiCH_2CH_2CH_2OH$, 8.2*H*), 1.73–1.80 (m, $SiCH_2CH_2CH_2OH$, 16.2*H*); 0.75–0.79 (m, $SiCH_2CH_2CH_2OH$, 16.3*H*). ^{13}C NMR (DMSO-d_6, ppm): 9.4 ($SiCH_2CH_2CH_2OH$), 26.6 ($SiCH_2CH_2CH_2OH$), 47.9 ($SiCH_2CH_2CH_2OH$). ^{29}Si NMR (ppm): −67.2.

2.4. Synthesis of star PCL

The ring-opening polymerization (ROP) of ε-caprolactone (CL) catalyzed by Stannous (II) octanoate [$Sn(Oct)_2$] was used to prepare the organic–inorganic star-shaped PCL. The ROP was carried out using a standard Schlenk line system. To a flask connected with the Schlenk line, octa(3-hydroxypropyl) POSS (0.20 g, 0.23 mmol), ε-caprolactone (4.1 g, 36 mmol) were charged into a 25 ml pre-dried flask and (4.1 mg, 0.01 mmol) of $Sn(Oct)_2$ was added as a catalyst. The reactive mixture was degassed *via* three pump freeze-thaw cycles and then immersed in a thermostated oil bath at 110 °C for 24 h. The crude products were dissolved with a smallest amount of CH_2Cl_2 and precipitated in an excessive amount of petroleum ether. This procedure was repeated for three times and the polymers were dried in a vacuum oven at 40 °C for 48 h. The results of polymerization are summarized in Table 1. ^1H NMR ($CDCl_3$, ppm): 3.5 ($SiCH_2CH_2CH_2$–PCL); 1.8 ($SiCH_2CH_2CH_2$–PCL); 0.79 ($SiCH_2CH_2CH_2$–PCL); 4.04–4.07 [−O−CO−$(CH_2)_4$−CH_2]; 2.28–2.32 [−O−CO−CH_2−$(CH_2)_4$]; 1.60–1.68 [−O−CO−$CH_2CH_2CH_2CH_2CH_2$]; 1.35–1.41, [−O−CO−CH_2−CH_2−CH_2−CH_2−CH_2].

Table 1
Results of polymerization for the star PCLs

Star PCLs	[CL]/[POSS]	$M_{n,th}$	M_n	M_w/M_n	Yield (%)
POSSPCL01	160:1	19,128	23,000	1.30	98.9
POSSPCL02	280:1	32,808	34,000	1.38	97.7
POSSPCL03	400:1	46,488	43,000	1.44	97.2
POSSPCL04	640:1	73,848	80,000	1.48	98.3
POSSPCL05	1280:1	146,808	130,000	1.50	96.9

2.5. Measurement and techniques

2.5.1. Nuclear magnetic resonance spectroscopy (NMR)

The NMR measurements were carried out on a Varian Mercury Plus 400 MHz NMR spectrometer at 27 °C. The samples were dissolved with deuteronated solvents and the NMR spectra were obtained with tetramethylsilane (TMS) as the internal reference. The solid-state NMR experiment was also carried out on the spectrometer. The high-resolution ^{29}Si NMR spectra were obtained using the cross polarization (CP)/magic angle spinning (MAS) together with the high-power dipolar decoupling (DD) technique. The 90°-pulse width of 4.6 μs was employed with free induction decay (FID) signal accumulation, and the CP Hartmann–Hahn contact time was set at 3.5 ms for all the experiments. The rate of MAS was 4.0 kHz for measuring the spectra. The Hartmann–Hahn CP matching and dipolar decoupling field was 57 kHz. The time of recycle delay was set to be 10.0 s for the signal accumulation. The chemical shifts of all ^{29}Si spectra were determined by taking the silicon of solid Q_8M_8 relative to TMS as an external reference standard.

2.5.2. Fourier transform infrared spectroscopy (FTIR)

The FTIR measurements were conducted on a Perkin–Elmer Paragon 1000 Fourier transform spectrometer at room temperature (25 °C). The sample films were prepared by dissolving the polymers with $CHCl_3$ (5 wt%) and the solutions were cast onto KBr windows. The residual solvent was removed in a vacuum oven at 60 °C for 2 h. The specimens were sufficiently thin to be within a range where the Beer–Lambert law is obeyed. In all cases 64 scans at a resolution of 2 cm^{-1} were used to record the spectra.

2.5.3. Gel permeation chromatography (GPC)

The molecular weights of the polymers were measured on a PE series 200 permeation chromatography (GPC) instrument with a PL mixed-B10m column. Polystyrene was used as the

standard, and THF was used as the eluent at a flow rate of 1 ml/min.

2.5.4. Wide-angle X-ray diffraction

The wide-angle X-ray diffraction (WAXRD) experiments were carried out on a Shimadzu XRD-6000 X-ray diffractometer with Cu K_α ($\lambda = 0.154$ nm) irradiation at 40 kV and 30 mA using a Ni filter. Data were recorded in the range of $2\theta = 10-60^\circ$ and step scanning mode was used with the step size of 0.02° and the preset time of 0.6 s.

2.5.5. Differential scanning calorimetry (DSC)

The calorimetric measurements were performed on a Perkin–Elmer Pyris 1 differential scanning calorimeter in a dry nitrogen atmosphere. The instrument was calibrated with standard Indium. The samples were firstly heated up to 100 °C at the heating rate of 20 °C/min and were held at 100 °C for 5 min to melt the crystals, followed by quenching to −70 °C. The second heating scans were carried out from −70 to 100 °C at the heating rate of 20 °C/min and the thermograms were recorded. After that, the samples were cooled from 100 to −70 °C at the cooling rate of 10 °C/min and the cooling DSC curves were recorded. Crystallization temperatures (T_c) and melting temperatures (T_m) were taken as the temperatures at maximum and the minimum of both endothermic and exothermic peaks, respectively.

Equilibrium melting points were measured by DSC. The samples were heated to 100 °C for 3 min to erase the thermal history, and then quenched to the desired temperature for isothermal crystallization toward completion. To measure the melting temperatures (T_ms) of the samples, the crystallized samples were heated at a heating rate of 10 °C/min and the T_ms were taken as the temperatures at which the crystals were totally molten. The overall crystallization kinetics from the melts was analyzed by differential scanning calorimetry. The samples were molten at 100 °C for 5 min to remove the thermal history, and then quenched to the desired temperatures at which the isothermal crystallization was allowed to carry out to completion, recording the isothermal thermographs. The conversion of crystallization, $X(t)$, as a function of crystallization time (t) was determined using the following equation:

$$X(t) = \int_0^t \left(\frac{dH}{dt}\right) dt \Big/ \int_0^\infty \left(\frac{dH}{dt}\right) dt \quad (1)$$

where the integral in the numerator is the enthalpy generated at time t and the integral in the denominator is the total enthalpy of crystallization at $t = \infty$. The observed melting temperature (T'_m) of the isothermally crystallized samples were measured by heating the samples from T_c up to 100 °C at a heating rate of 10 °C/min.

3. Results and discussion

3.1. Synthesis of octa(3-hydroxypropyl) POSS

The synthetic route of the organic–inorganic star-shaped PCL with POSS core is described in Scheme 2. It is mandatory to prepare the POSS core molecule with eight equivalent hydroxyl groups. It has been proposed that octa(3-hydroxylpropyldimethylsiloxy)octasilsesquioxane can be prepared *via* the hydrosilylation between octakis(dimethylsiloxy) octasilsesquioxane ($Q_8M_8^H$) and allyl alcohol. Nonetheless, both C- and O-silylation could be involved with the direct hydrosilylation. Zhang and Laine [48] found that the utilization of Karstedt catalyst can give the cleanest C-silylation. Therefore, the utilization of bulky protective groups such as *tert*-butyldimethylsilyl chloride (TBDMS) [46] connected to allyl alcohol was necessary to minimize the occurrence of *O*-silylation. Nonetheless, the backbiting problem must be considered for desilylation in certain solvents [48]. In the present work, we proposed a novel and facile approach to prepare octa(3-hydroxypropyl) POSS molecules without using the method of hydrosilylation.

In the present work, the starting compound for preparing octa(3-hydroxypropyl) POSS is octa(3-chloropropyl) POSS, which was synthesized with a good yield *via* the hydrolytic condensation of 3-chloropropyltrimethoxysilane as described by Dittmar et al. [47]. The readily available octa(3-chloropropyl) POSS was further used to afford octa(3-hydroxypropyl) POSS. The nucleophilic substitution of chlorine atoms by hydroxyl groups was used to achieve the transformation of octa(3-chloropropyl) POSS into octa(3-hydroxypropyl) POSS. The reaction of the nucleophilic substitution was carried out in the mixture of tetrahydrofuran and stoichiometric amount of water with respect to the quantity of chloropropyl groups in the presence of freshly prepared silver oxide (Ag_2O) to proceed the reaction to completion. It should be pointed out that some basic systems such as aqueous sodium carbonate (Na_2CO_3) and sodium hydroxide (NaOH) were not used to convert the halogenated hydrocarbon groups into alkyl alcohol since the rearrangement of octa(3-chloropropyl) POSS cages could occur [49]. Shown in Fig. 1 is the ^{1}H NMR spectrum of the octa(3-hydroxypropyl) POSS. It is seen that

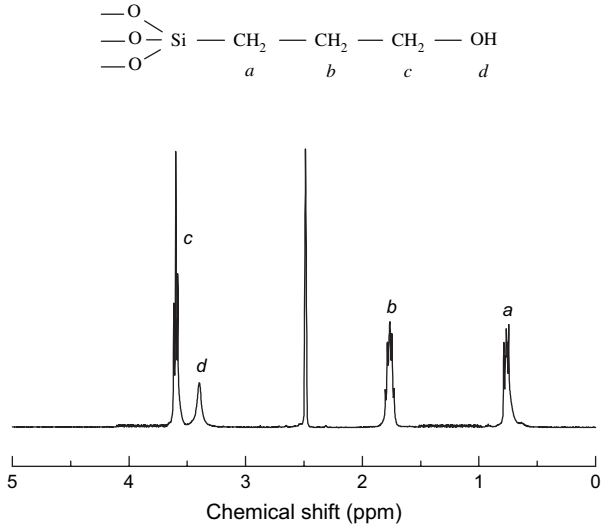

Fig. 1. The ^{1}H NMR spectrum of octa(3-hydroxypropyl) POSS.

the resonance of hydroxyl protons occurs at 3.38 ppm. In terms of the ratio of the integration intensity of proton resonance of hydroxyl groups at 3.38 ppm to those of methylene protons, it is judged that the conversion of the C–Cl into C–OH moieties was performed to completion. The solid-state ^{29}Si NMR spectra of octa(3-chloropropyl) and octa(3-hydroxypropyl) POSS are presented in Fig. 2. For octa(3-chloropropyl) POSS, two signals of resonance were seen at −65.6 and −66.3 ppm, respectively, which are ascribed to the resonance of Si nucleus in the crystalline and noncrystalline region. The fact that only single resonance at −67.2 ppm was detected in the ^{29}Si NMR spectrum indicates that the cage-arrangement of silsesquioxane did not occur under the present condition of reaction. Therefore, the octa(3-hydroxypropyl) POSS was successfully obtained.

3.2. Synthesis of PCL stars with POSS core

Under appropriate conditions for a living/controlled polymerization, the ring-opening polymerization (ROP) of lactone is efficient for preparing polyester with desired molecular weight and narrow molecular weight polydispersity. Depending on the number of initiator functionality molecules, the star PCLs with various number of arms can be obtained [25,29–31]. In this work, octa(3-hydroxypropyl) POSS was an octafunctional initiator, and stannous (II) octanoate [$Sn(Oct)_2$] was used as the catalyst to prepare the octaarmed star PCL with POSS core. By controlling the molar ratios of octa(3-hydroxypropyl) POSS to ε-caprolactone (CL), a series of star PCLs with various arm lengths (or POSS contents) were obtained. Representatively shown in Fig. 3 is the ^{1}H NMR spectrum of POSSPCL02 sample together with the assignment of the spectrum. The resonances of the $-CH_2-$ moiety in POSS core are discernible in the NMR spectrum, indicating the presence of POSS cores in the star PCL.

The star PCL samples were subjected to gel permeation chromatography (GPC) measurements and the results of polymerization are summarized in Table 1. It is seen that the conversion is almost complete under the present condition,

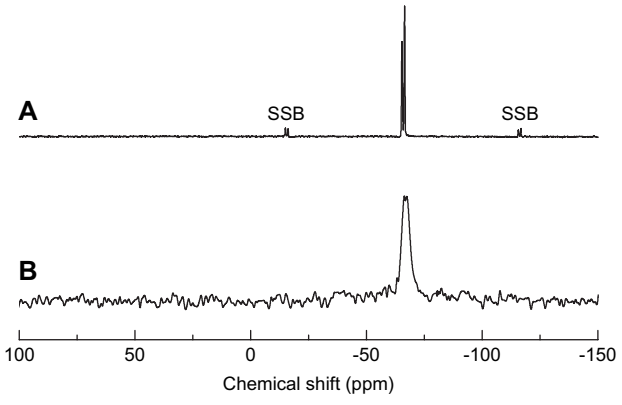

Fig. 2. The ^{29}Si NMR spectra of octa(3-chloropropyl) POSS (A) and octa(3-hydroxypropyl) POSS (B).

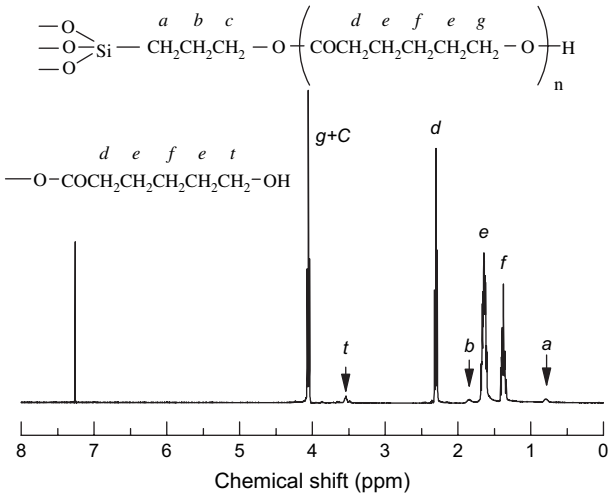

Fig. 3. The representative NMR spectra of the star PCL (*viz*. POSSPCL02).

indicating that the octafunctional POSS molecule is an efficient initiator. Fig. 4 presents the plots of molecular weight and polydispersity as a function of the molar ratio of [CL] to [POSS]. It is seen that the average molecular weight (M_n) of the products linearly increased with increasing the molar ratio of monomer to initiator whereas the molecular weight polydispersity slightly increased. This observation suggests that the molecular weight of the star PCL can be controlled in terms of the ratios of monomer to initiator. It should be pointed out that the determination of molecular weight for the star PCL by means of gel permeation chromatography (GPC) could be subject to some underestimation due to the characteristics of lower hydrodynamic volume for star-like or branched macromolecules.

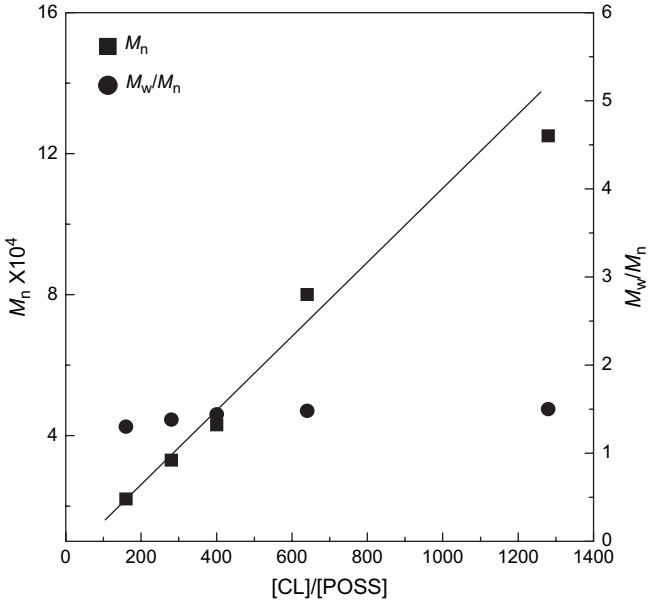

Fig. 4. The plots of molecular weight and polydispersity for the star PCLs as a function of the ratio of [CL] to [POSS].

3.3. Characterization of star PCL with POSS core

3.3.1. Crystalline structure

The wide-angle X-ray diffraction (WAXRD) measurements between 10° and 50° were employed to examine the crystalline structure of the POSS-containing star PCLs. The diffraction patterns of POSS-containing PCLs (*viz*. POSSPCL01 and POSSPCL03) are shown in Fig. 5. For comparison, the XRD curve of control linear PCL was also incorporated in this figure, which was measured with the identical condition. The diffraction peak positions of linear PCL agree well with the reported unit cell parameters for PCL (orthorhombic, $a = 7.47$ Å, $b = 4.98$ Å, $c = 17.05$ Å) [50]. The intense diffraction peaks located at $2\theta = 21.39°$, 22.00°, 23.70°, corresponding to the (110), (111) and (200) reflections [51] of PCL were observed for the linear PCL. For the POSS-containing star PCL, it is seen that the diffraction peaks at $2\theta = 21.39°$, 22.00° and 23.70° remained invariant in comparison with the linear PCL. This observation suggests that there was little change in the crystalline structure for the POSS-containing star PCL. Therefore, the presence of POSS core did not alter the packing structure of PCL chains in the crystals [52–54]. It should be pointed out that the diffraction peak at 43.99° is ascribed to the (200) reflection of aluminum (*i.e*., the sample holder), which remained invariant for the different samples.

3.3.2. Thermal properties

With the identical thermal history being applied to the samples, the heating DSC thermograms for the linear and star PCLs are shown in Fig. 6. All the star PCL samples displayed the melting transitions at *ca*. 56 °C as control PCL, indicating that the organic–inorganic star PCLs were crystallizable. It is noted that the star PCLs with the higher arm lengths (*e.g*., POSSPCL03, POSSPCL04 and POSSPCL05) displayed the higher melting temperatures than the linear PCL whereas those with the lower arm lengths (*viz*. POSSPCL01 and POSSPCL02) exhibited the lower temperatures than the control PCL. This observation was further confirmed by the measurements of equilibrium melting points. Shown in Fig. 7 are the plots of T'_m as a function of crystallization temperature (T_c) for the linear and star PCLs in a wide range of undercooling. The equilibrium melting points (T^0_m) are determined by extrapolation to the lines of $T_m - T_c$ according to the Hoffman–Weeks equation [55,56]:

$$T'_m = \Phi T_c + (1 - \Phi) T^0_m \quad (2)$$

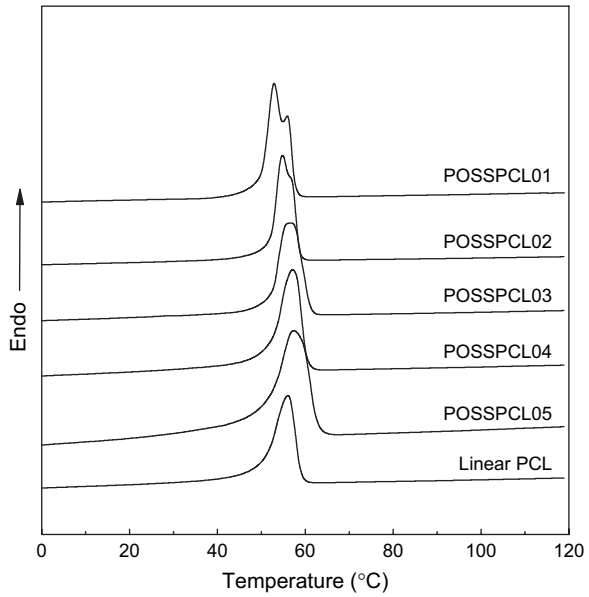

Fig. 6. The heating DSC thermograms of the linear and star PCL of various molecular weights (second scans).

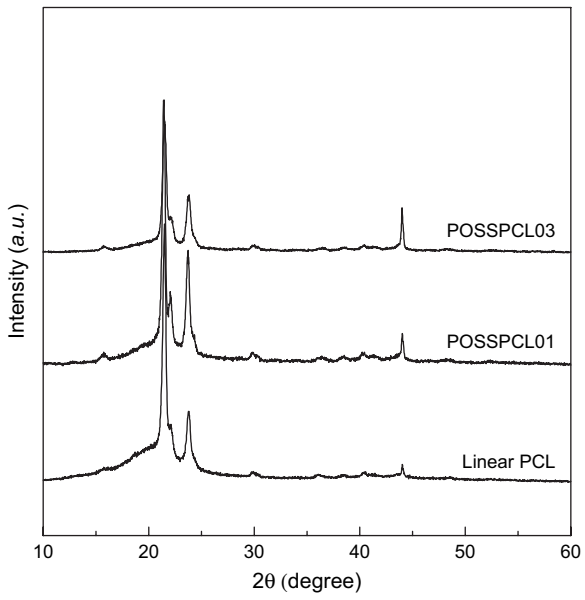

Fig. 5. The XRD curves of linear PCL and the star PCL (i.e., POSSPCL01 and POSSPCL03).

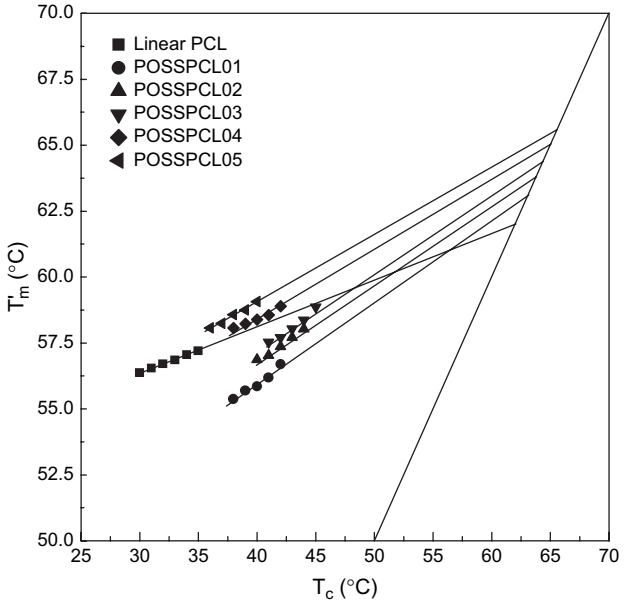

Fig. 7. Hoffman–Weeks plots for the determination of equilibrium melting points.

where Φ is a stability parameter and T_m the apparent melting temperature. The value of Φ is between 0 ($T_m = T_m^0$ for all T_c, in the case of most stable crystal) and 1 ($T_m = T_c$ in the case of inherently unstable crystal). The Φ parameters can be obtained from the slope of the straight lines and the values of T_m^0 were determined by extrapolating the least-squares fit lines of the experimental data according to Eq. (2) to intersect the line of $T_m = T_c$ as shown in Fig. 7. The T_m^0 together with Φ parameters are summarized in Table 2. The value of Φ was 0.17 for the linear PCL whereas the values of 0.26–0.35 were obtained for these star PCLs investigated. In terms of the stability parameter, it is judged that the star-shaped PCL crystals are less stable than the linear PCL crystals. There could be two factors to affect the stability of crystals. On the one hand, the chain length of PCL arms in the star PCL is much shorter than that of the linear PCL, *i.e.*, the short PCL arms could be hard to develop stable crystals. On the other hand, the stability of crystals in the star PCL could be restricted by the POSS cores. The core effect is more pronounced for the PCL stars with shorter arms. Nonetheless, it is still accepted that the PCL crystals in the star polymers are still fairly stable after the POSS molecules were incorporated. It is noted that all the PCL stars displayed enhanced equilibrium melting points (T_m^0) and the values of (T_m^0) increased with increasing the arm lengths. The results of equilibrium melting points are in good agreement with those of kinetic melting temperatures. The melting behavior of the organic–inorganic star PCLs is in marked contrast to those of the star crystalline polymers with organic cores [52,53] and that of cage-like fullerene (C_{60})-end-capped poly(ethylene oxide) [55]. The increased (T_m^0) for the PCL stars could be ascribed to the positional restriction imposed on the PCL chains by their covalent attachment to the POSS core, which reduces the melt entropy of the star polymers with respect to their linear analogues [32,52–55]. It should be pointed out that the decreased melting points for the samples with the shorter arms (*e.g.*, POSSPCL01) could be ascribed to the lower ability to crystallize the shorter PCL arm (*ca.* 3000). It is difficult to develop a thick enough crystal in the PCL stars with the shorter arms of PCL arms, owing to the restriction of the chain movement of PCL arms by the POSS core compared to the linear PCL. In addition, it is noted that for the PCL stars (*viz.* POSSPCL01 and POSSPCL02), the dual melting transitions were observed under the commonly used heating rate, 20 °C/min for the quenched samples (Fig. 6). The dual melting behavior of PCL is attributed to melting of the initial crystals followed by recrystallization and final melting of the crystals grown during the heating scan [57]. The fact that the dual melting transitions for POSSPCL01 and POSSPCL02 occurred even during the fast heating process implies that the crystallization rearrangement was slowed down by the formation of the star-shaped topological structure.

Table 2
Equilibrium melting points T_m^0 and stability parameters (Φ)

Samples	T_m^0 (°C)	Φ
POSSPCL01	63.1	0.36
POSSPCL02	63.8	0.34
POSSPCL03	64.4	0.33
POSSPCL04	65.0	0.26
POSSPCL05	65.6	0.26
Linear PCL	62.0	0.17

Fig. 8 presents the cooling DSC thermograms of the linear and star PCLs. It is seen that the crystallization temperatures (T_c) of the PCL stars are much higher than that of control PCL. For the PCL stars, the T_c increases with increasing the percentage of POSS core in the samples; the T_c of the star PCLs with the very high molecular weight (*e.g.*, POSSPCL05) was even close to that of the linear PCL. The enhanced crystallization temperatures suggest that the crystallization of chains in the POSS-containing star PCLs is faster than in the linear counterpart of PCL. It is proposed that there could be two competitive factors to affect the crystallization behavior of macromolecular chains of the star PCL depending on the molecular weight (*viz.* POSS contents). The first one is related to the macromolecular topological effect. For the star PCLs, the crystalline arms were covalently bound onto the nanosized cubic silsesquioxane cages through the ester linkages. The topological structure could constitute an obstacle to crystallization arrangement as in hyperbranched or other star-like crystalline polymers, which have been evidenced by the appearance of the dual melting transition in the heating DSC scan, and thus reduce the rate of crystallization [32,51]. The second effect is connected with the heterogeneous nucleating effect of POSS cores. In the organic–inorganic hybrid composite system, the inorganic octameric cubic POSS molecules could act as the heterogeneous nucleating agent to accelerate the crystallization of PCL. For the star PCLs with the shorter arms the first factor dominates, which was evidenced by the appearance of the dual melting transitions and the depression

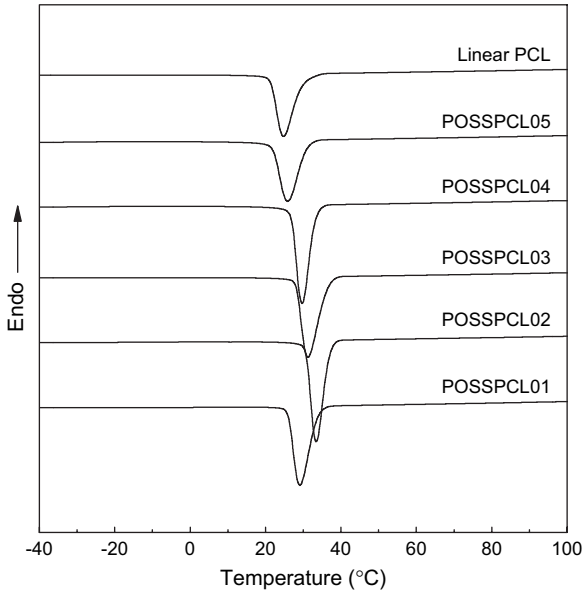

Fig. 8. The cooling DSC thermograms of the linear and star PCLs at the rate of −10 °C/min.

in melting points in terms of the heating DSC scans. It should be pointed out that the observation that the star PCL with the shorter arms (*e.g.*, POSSPCL01) displayed the lower crystallization temperature than other star PCLs could be interpreted based on the confinement effect of star-like topological structure and the effect of short arms on the crystallization. From the results presented in Figs. 6–8, it is plausible to propose that the nucleating effect of POSS cores dominates the process of crystallization for the samples with the longer arms.

Returning to Fig. 6, the crystallinity of the star PCLs can be calculated from the heat DSC curves using the following equation:

$$X_c = \frac{\Delta H_c}{\Delta H_f^0} \times 100\% \quad (3)$$

where ΔH_c is the fusion enthalpy of the re-scanned samples after quenching from the melts and ΔH_f^0 is the fusion enthalpy of the perfectly crystallized PCL and equals 136 J/g [52]. Fig. 9 shows the plot of crystallinity as a function of molecular weight for the linear and star-shaped PCLs. The star PCLs showed a depression in crystallinity with respect to PCL. The decreased crystallinity reflects the difference in the ability to crystallize between the linear and the star PCLs. It is noted that the crystallinity of the star PCLs increased with increasing the length of PCL arms and is close to that of the linear PCL.

3.4. Isothermal crystallization kinetics

3.4.1. Analysis of Avrami equation

Representatively shown in Fig. 10 are the plots of the conversion of crystallization as functions of time for POSSPCL02. It can be seen that with increasing crystallization temperature, the characteristic sigmoid $X(t) - t$ curves are significantly shifted to the right side along the time axis, suggesting that crystallization processes become progressively slow and also indicating that nucleation is a rate-controlling step under the present conditions of crystallization. From the curves, the times of half-crystallization $t_{1/2}$, defined as the time required for half of the crystallinity to develop were obtained. The plots of $t_{1/2}$ as functions of T_c for various samples are shown in Fig. 11. It is seen that at a given T_c, the overall crystallization rates of the star PCLs decreased with increasing the molecular weight of the star PCL, *i.e.*, the crystallization becomes faster with inclusion of POSS. It should be pointed out that the lower crystallization rate for POSSPCL01 could result from its

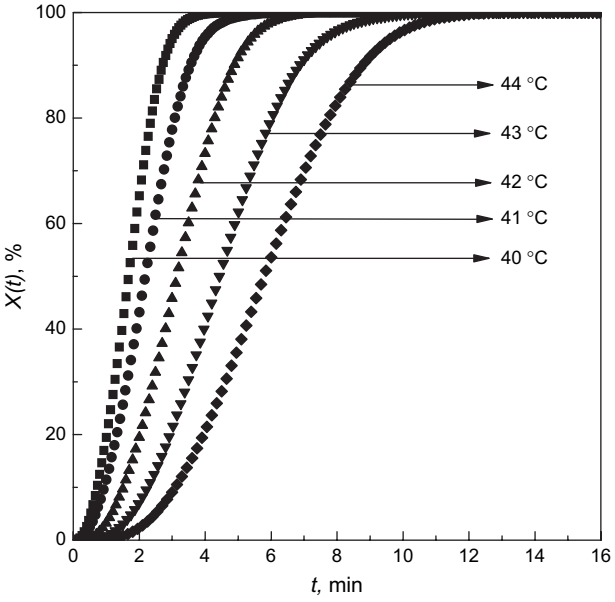

Fig. 10. The representative plots of the conversion of crystallization as functions of time for a star PCL (*viz*. POSSPCL02).

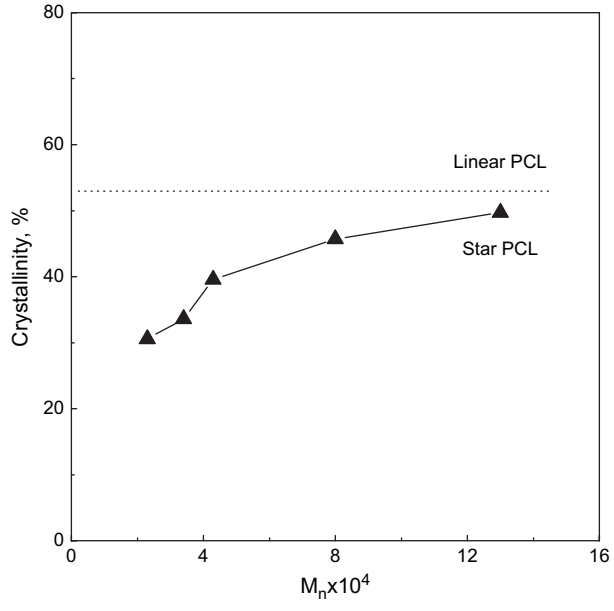

Fig. 9. The plot of crystallinity for the linear and star PCLs as a function of molecular weight.

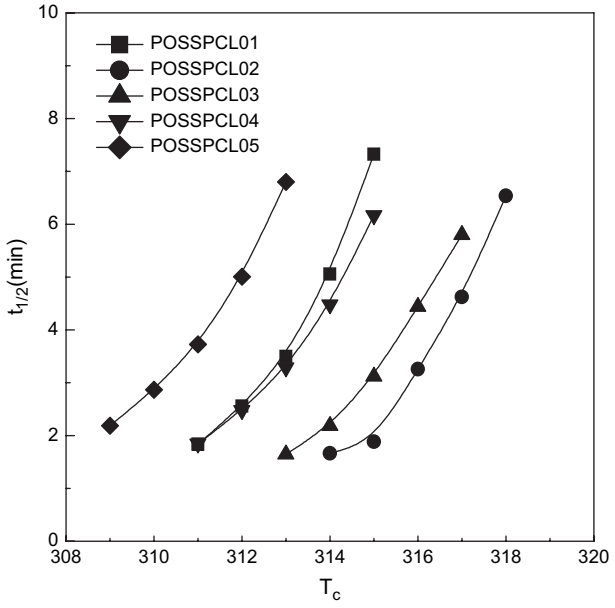

Fig. 11. The plots of $t_{1/2}$ as functions of T_c for various samples.

shorter PCL arms. As well known, the overall crystallization rate is determined by the rates of both growth and nucleation. In the present case, the fact that overall crystallization rates increased with the incorporation of POSS could be related to the changes in nucleation rate (or mechanism) for the star PCLs, *i.e.*, the POSS cores could act as the heterogeneous nucleating agent to accelerate the rate of nucleation.

The kinetics of isothermal crystallization was analyzed using Avrami equation [59]:

$$X_t = 1 - \exp(-K_n t^n) \tag{4}$$

where K_n is the overall kinetic rate constant and n is Avrami index that depends on the type of nucleation and on the geometry of growing crystals. The values of K_n and n were obtained from the intercept and the slope of the linear plots of $\log[-\ln(1 - X(t))]$ as a function of $\log t$ (Fig. 12). The experimental results are well coincident with the linear relation for the early part of the transformation. Generally, Avrami equation is usually only valid at low conversion of crystallization as long as the impingement is not serious [57,60,61]. The values of K_n, n, $t_{1/2}$ and T_m^0 are summarized in Table 3. For the control PCL, the n values obtained were in the vicinity of 4.0, suggesting a three-dimensional growth of crystalline units, *i.e.*, the crystallization process is developed by heterogeneous nucleation in the sample. It is noted that the n values significantly increased the inclusion of POSS. Depending on the arm lengths of the PCL stars the n values varied from 4.0 to 5.2, implying the branching mechanism of macromolecular crystals [62].

3.4.2. Overall kinetic rate constants (K_n)

The spherulitic growth kinetics of the star PCLs can be analyzed according to Hoffman–Lauritzen crystallization kinetic theory [62–64]. The dependence of the growth rate G on crystallization temperature T_c and on undercooling ($\Delta T = T_m^0 - T_c$) is accounted for by the following equation [55]:

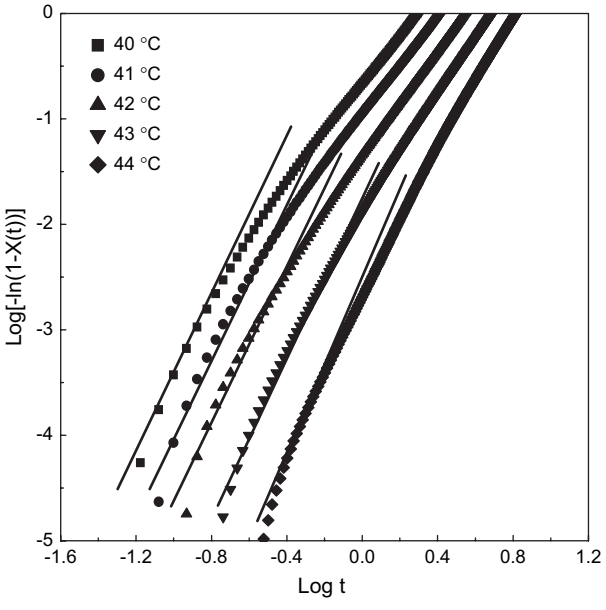

Fig. 12. The linear plots of $\log[-\ln(1 - X(t))]$ as a function of $\log t$.

Table 3
Values of $t_{1/2}$, K_n, n, and T'_m at various T_cs

PCL	T_c (°C)	T'_m (°C)	$t_{1/2}$ (min)	K_n (min^{-n})	n
Linear PCL	304	329.5	1.34	3.66×10^{-2}	4.1
	305	329.7	2.56	1.64×10^{-3}	4.0
	306	329.9	3.74	2.47×10^{-4}	3.9
	307	330.0	4.92	1.65×10^{-3}	3.8
	308	330.2	6.26	4.19×10^{-5}	4.2
POSSPCL01	311	328.4	1.84	1.04×10^{-6}	4.8
	312	328.7	2.56	3.08×10^{-6}	5.2
	313	328.9	3.50	2.33×10^{-5}	5.1
	314	329.2	5.06	1.42×10^{-4}	4.8
	315	329.7	7.33	7.16×10^{-4}	4.9
POSSPCL02	313	329.9	1.67	3.33×10^{-7}	4.5
	314	330.0	1.89	9.67×10^{-7}	4.7
	315	330.4	3.26	2.10×10^{-6}	5.1
	316	330.7	4.63	7.44×10^{-5}	4.9
	317	331.0	6.54	2.30×10^{-3}	4.7
POSSPCL03	314	330.5	1.65	3.00×10^{-6}	4.9
	315	330.7	2.19	7.33×10^{-5}	4.0
	316	331.0	3.12	1.10×10^{-4}	4.7
	317	331.3	4.44	4.53×10^{-3}	4.1
	318	331.9	5.80	5.35×10^{-2}	4.4
POSSPCL04	311	331.1	1.85	5.22×10^{-5}	4.4
	312	331.2	2.48	3.59×10^{-4}	4.2
	313	331.4	3.29	2.24×10^{-3}	4.1
	314	331.6	4.48	7.44×10^{-3}	4.3
	315	331.9	6.17	8.02×10^{-2}	4.0
POSSPCL05	309	331.1	2.19	1.40×10^{-4}	3.9
	310	331.2	2.87	3.47×10^{-4}	4.4
	311	331.6	3.73	1.08×10^{-3}	4.0
	312	331.7	5.01	3.84×10^{-3}	4.0
	313	332.1	6.80	1.19×10^{-2}	3.8

$$G = \Phi_2 G_0 \exp\left[-\frac{\Delta F^*}{RT_c}\right] \exp\left[-\frac{K_g}{fT_c\Delta T} + \frac{2\sigma_u T_m^0 \ln \Phi_2}{b_0 \Delta H v \Delta T}\right] \tag{5}$$

$$f = \frac{2T_c}{T_m^0 + T_c} \tag{6}$$

$$K_g = \frac{Z b_0 \sigma \sigma_e T_m^0}{k \Delta H_f^0} \tag{7}$$

where G_0 is a pre-exponential factor, generally assumed to be a constant or proportional to T_c; ΔF^* represents the sum of the activation energies for the chain motion in the melt. R is the gas constant and k is the Boltzmann constant. Φ_2 is the volume fraction of crystalline polymer. The quantity f is the correction factor for the enthalpy of fusion. K_g is the nucleation factor; b_0 the layer thickness; $\Delta H_f^0 = 136$ J/g [58] is the theoretical enthalpy of fusion per unit mass; σ and σ_e, the surface energies of lateral and extremity surfaces, respectively; and Z, a coefficient that depends on the growth regime, $Z = 4$ in regimes I and III and $Z = 2$ in regime II [66,67].

The transport term ΔF^* in Eq. (5) may be estimated with a satisfactory precision using WLF equation [68]:

$$\Delta F^* = \frac{C_1 T_c}{C_2 + T_c - T_g} \tag{8}$$

where C_1 and C_2 are constants (generally assumed as 4120 cal/J and 51.5 K, respectively) and T_g the glass transition temperature.

For the overall crystallization rate, we used $G = CK_n^{1/n}$, where C is a constant. Assuming $\sigma = 0.1 b_0 \Delta H_f^0$ [65,69] and taking into account the relations (6) and (7), the above expression may be re-organized as:

$$f(K_n) = \frac{1}{n}\ln K_n - \ln \Phi_2 + \frac{C_1}{R(C_2 + T_c - T_g)} - \frac{0.2 T_m \ln \Phi_2}{\Delta T} = \log A_0 - \frac{K_g}{f T_c \Delta T} \tag{9}$$

By plotting the quantity $f(K_n)$ against $1/(f T_c \Delta T)$, the linear plots are shown in Fig. 13 for the various samples. For all samples, single slopes are evident in the range of T_c investigated, indicating single regime. Herewith, regime II growth kinetics was employed to estimate the folding free energy of surface (σ_e). From the slopes and the intercepts of these lines, values of the free surface energy of folding σ_e and pre-exponential factors A_0 were calculated by using $b_0 = 4.38 \times 10^{-8}$ cm. The results are summarized in Table 4, it can be seen that for the star PCL, the A_0 showed the molecular weight dependence and increased with increasing the POSS content, *i.e.*, A_0 increased with decreasing the molecular weight of the star PCL. Fig. 14 presents the plot of the values of σ_e as a function of the molecular weight of the star PCL. The values of $\sigma_e = 0.041–0.093$ J/m^2 for the star PCLs in this work are intermediate between the lower values obtained by Ong and Price [60] (0.027 J/m^2) and the higher values obtained by Goulet and Prud'homme [70] (0.112 J/m^2). It is seen that the values of σ_e decreased with increasing the content of POSS, (or with decreasing the molecular weights of the star PCLs). This observation could be interpreted in terms of the combination of the surface enthalpy and entropy of folding ($\sigma_e = H_e - TS_e$) [60]. It is expected that in the star-shaped PCLs, the covalent attachment of the PCL arms to the cubic POSS cores could restrict the positional freedom and thus the entropy of folding (S_e) will decrease with respect to that of linear PCL. It is plausible to propose that the entropy of folding (S_e) is not favorable for the decrease in the folding free energy of surface (σ_e) for the star PCLs. Therefore, the enthalpic contribution (H_e) to σ_e might be significant to affect the folding free energy of surface. In the present case, the change in folding enthalpy could be associated with the change of crystalline structure posed by the inorganic POSS cores, which was evidenced by the results of XRD. It is noted that the values of σ_e increase with increasing the molecular weight of PCL arms, implying that effect of POSS cores is not so significant for the star PCLs with the high molecular weights. It is interesting to note that the results of σ_e are

Table 4
Values of A_0, K_g and σ_e

PCLs	A_0	K_g (K^2)	σ_e (J/m^2)
POSSPCL01	1.30×10^9	4.84×10^4	4.12×10^{-2}
POSSPCL02	5.72×10^{11}	6.48×10^4	5.32×10^{-2}
POSSPCL03	7.51×10^{11}	6.85×10^4	6.30×10^{-2}
POSSPCL04	3.00×10^{13}	8.93×10^4	7.50×10^{-2}
POSSPCL05	4.23×10^{14}	10.6×10^4	9.29×10^{-2}
Linear PCL	1.79×10^{10}	6.22×10^4	5.68×10^{-2}

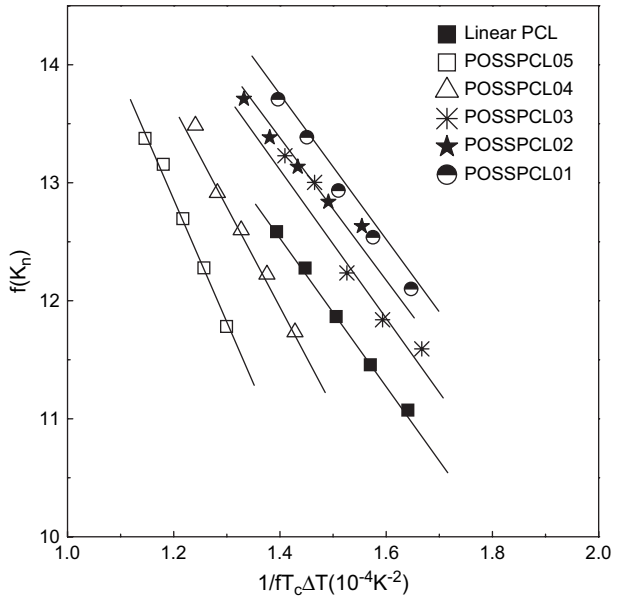

Fig. 13. The plots of the quantity $f(K_n)$ against $1/(f T_c \Delta T)$.

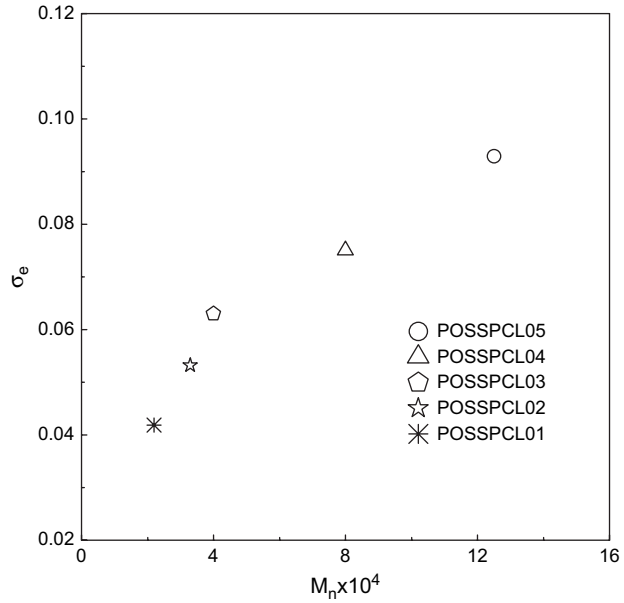

Fig. 14. The plots of the values of σ_e as a function of the molecular weight of the star (and/or linear) PCL.

coincident with the observation that the inorganic POSS cores act as the heterogeneous nucleating agent to facilitate the process of crystallization.

4. Conclusions

In this study, we reported a facile approach to prepare a novel octa(3-hydroxypropyl) POSS, which was used as an octafunctional initiator for the synthesis of the octaarmed star-shaped PCLs. The organic–inorganic star PCLs with various degree of polymerizations were synthesized *via* ring-opening polymerization catalyzed by stannous (II) octanoate [$Sn(Oct)_2$]. The star PCLs were characterized by means of gel permeation chromatography (GPC), Fourier transform infrared spectroscopy (FTIR) and nuclear magnetic resonance spectroscopy (NMR). The wide-angle X-ray diffraction (WAXRD) experiments indicate that the presence of POSS cores did not alter PCL crystal structure. The star PCLs displayed the equilibrium melting points higher than the linear counterpart. Both the overall crystallization rate and the spherulitic growth rate of the star PCLs increased with increasing the concentration of POSS (or with decreasing the molecular weights of the star PCLs). It is found that the folding free energy of surface for the star PCLs decreased with increasing the concentration of POSS. These results could be ascribed to the effect of the favorable heterogeneous nucleation of POSS cores, which accelerates the process of crystallization.

Acknowledgments

The financial support from Shanghai Science and Technology Commission, China under a key project (No. 02DJ14048) was acknowledged. The authors would also like to acknowledge Natural Science Foundation of China (Project No. 20474038 and 50390090) and Shanghai Educational Development Foundation, China under an award (2004-SG-18) to ''Shuguang Scholar'' for the partial support.

References

[1] Hadjichristidis N. J Polym Sci Part A Polym Chem 1999;37:857.
[2] Misha MK, Kobayashi S, editors. Star and hyperbranched polymers. New York: Marcel Dekker; 1999.
[3] Alward DB, Kinning DJ, Thomas EL, Fetters LJ. Macromolecules 1986; 19:21.
[4] Tselikas Y, Hadjichristidis N, Lescanec RL, Honeker CC, Wohlgemuth M, Thomas EL. Macromolecules 1996;29:3396.
[5] Wei J, Huang J. Macromolecules 2005;38:1107.
[6] Costa RD, Vasconcelos WL, Tamaski R, Laine RM. Macromolecules 2001;34:5398.
[7] Maitra P, Wunder SL. Chem Mater 2002;14:4494.
[8] Kasko AM, Heintz AM, Pugh C. Macromolecules 1998;31:256.
[9] Ueda J, Matsuyama M, Kamigaito M, Sawamoto M. Macromolecules 1998;31:557.
[10] Ueda J, Kamigaito M, Sawamoto M. Macromolecules 1998;31:6762.
[11] Angot S, Murthy KS, Taton D, Gnanou Y. Macromolecules 1998;31: 7218.
[12] Matyjaszewski K, Miller PJ, Pyun J, Kickelbick G, Diamant IS. Macromolecules 1999;32:6562.
[13] Ohno K, Wong B, Haddleton DM. J Polym Sci Part A Polym Chem 2001;39:2206.
[14] Narrainen AP, Pascual S, Haddleton DM. J Polym Sci Part A Polym Chem 2002;40:429.
[15] Se K, Inoue N, Yamashita M. Polymer 2005;46:9753.
[16] Deng G, Gao M, Huang J, He L, Chen Y. Polymer 2005;46:5698.
[17] Zhao Y, Chen Y, Chen C, Xi F. Polymer 2005;46:5808.
[18] Kowalczuk-Bleja A, Trzebicka B, Komber H, Voit B, Dworak A. Polymer 2004;45:9.
[19] Stenzel-Rosenbaum M, Davis TP, Chen V, Fane AG. J Polym Sci Part A Polym Chem 2001;39:2777.
[20] Hou S, Chaikof EL, Taton D, Gnanou Y. Macromolecules 2003;36:3874.
[21] Hou S, Taton D, Saule M, Logana J, Chaikof EL, Gnanou Y. Polymer 2003;44:5067.
[22] Degh P, Dubois P, Jerome R, Teyssie P. Macromolecules 1992;25:4242.
[23] Dong T, Dubois P, Jerome R, Teyssie P. Macromolecules 1994;27:4134.
[24] Heise A, Trollsas M, Magbitang T, Hedrick JL, Frank CW, Miller RD. Macromolecules 2001;34:2798.
[25] Trollsa M, Hedrick JL. J Am Chem Soc 1998;120:4644.
[26] Liu YC, Ko BT, Lin CC. Macromolecules 2001;34:6196.
[27] Martin O, Averous L. Polymer 2001;42:6209.
[28] Jeong B, Bae YH, Lee DS, Kim SW. Nature (London) 1997;388:860.
[29] Dong CM, Qiu KY, Gu ZW, Feng XD. Macromolecules 2001;34:4691.
[30] Dong CM, Qiu KY, Gu ZW, Feng XD. Polymer 2001;42:6891.
[31] Choi J, Kim I-K, Kwak S-Y. Polymer 2005;46:9725.
[32] Núñez E, Ferrando C, Malmström E, Claesson H, Werner P-E, Gedde UW. Polymer 2004;45:5251.
[33] Agaska PA. Colloids Surf 1992;63:131.
[34] Voronkov MG, Lavrent'ev V. Top Curr Chem 1982;102:199.
[35] Feher FJ, Soulivong D, Eklund AG. Chem Commun 1998;399.
[36] Hoebbel D, Pitsch I, Reiher T, Hiller W, Jancke H, Muller D. Z Anorg Allg Chem 1989;576:160.
[37] Weidner R, Zeller N, Deubzer B, Frey V. US Patent 5 047 492; 1991.
[38] Schwab JJ, Lichtenhan JD. Appl Organomet Chem 1998;12:707.
[39] Li G, Wang L, Ni H, Pittman CU. J Inorg Organomet Polym 2001;11: 123.
[40] Matsuura Y, Matsukawa K, Kawabata R, Higashi N, Niwa M, Inoue H. Polymer 2002;43:1549.
[41] Ogoshi T, Chujo Y. Compos Interface 2005;11:539.
[42] Wang YW, Yen CT, Chen WC. Polymer 2005;46:6959.
[43] Kalogeras IM, Neagu ER. Eur Phys J 2004;E14:193.
[44] Choi M, Kleitz F, Liu DN, Lee HY, Ahn WS, Ryoo R. J Am Chem Soc 2005;127:1924.
[45] Sung YT, Kum CK, Lee HS, Byon NS, Yoon HG, Kim WN. Polymer 2005;46:5656.
[46] Chan S-C, Kuo S-W, Chang F-C. Macromolecules 2005;38:3099.
[47] Dittmar U, Hendan JB, Floerke U, Marsmann HC. J Organomet Chem 1995;489:185.
[48] Zhang C, Laine RM. J Am Chem Soc 2000;122:6979.
[49] Rikowski E, Marsmann HC. Polyhedron 1997;16:3357.
[50] Hu H, Dorset DL. Macromolecules 1990;23:4604.
[51] Nojima S, Hashizume K, Rohadi A, Sasaki S. Polymer 1997;38:2711.
[52] Chen E-Q, Lee S-W, Zhang A, Moon B-S, Man I, Harris FW, et al. Macromolecules 1999;32:4784.
[53] Floudas G, Reiter G, Lambert O, Dumas P. Macromolecules 1998;31: 7279.
[54] Zhao Y-L, Cai Q, Jiang J, Shuai X-T, Bei J-Z, Chen C-F, et al. Polymer 2002;43:5819.
[55] Hoffman JD, Weeks JJ. J Chem Phys 1962;37:1723.
[56] Hoffman JD, Weeks JJ. J Res Natl Bur Stand (US) Sect A 1962;66:13.
[57] Wundlich B. Macromolecular physics, vols. 1–3. London: Academic Press; 1973–1980.
[58] Crescenzi V, Manzini G, Calzolari G, Borri C. Eur Polym J 1972;8: 449.
[59] Avrami M. J Chem Phys 1941;9:177.
[60] Ong CJ, Price FT. J Polym Sci Polym Symp 1978;63:59.
[61] Morgan LB. Phil Trans Roy Sci (London) 1954;247:13.
[62] Hoffman JD. Soc Plast Eng Trans 1960;4:315.

[63] Hoffman JD, Frolen LJ, Ross GS, Lauritzen JI. J Res Natl Bur Stand (US) 1975;79A:671.
[64] Hoffman JD. Polymer 1983;24:3.
[65] Boon J, Azcue JM. J Polym Sci Part A2 1968;6:885.
[66] Defieuw G, Groeninckx G, Reynaers H. Polymer 1989;30:2164.
[67] Rim PB, Runt JP. Macromolecules 1983;16:762.
[68] William ML, Landel RF, Ferry JD. J Am Chem Soc 1955;77:3701.
[69] Thomas DG, Stavely IAK. J Chem Soc 1962;4569.
[70] Goulet L, Prud'homme RE. J Polym Sci Part B Polym Phys 1990;28:2329.